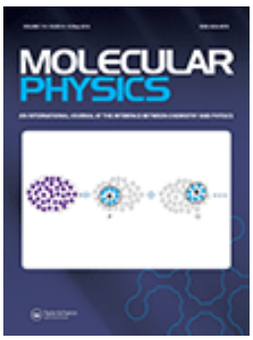

Taylor & Francis
Taylor & Francis Group

Molecular Physics

An International Journal at the Interface Between Chemistry and Physics

ISSN: 0026-8976 (Print) 1362-3028 (Online) Journal homepage: https://www.tandfonline.com/loi/tmph20

Isotope shifts and band progressions in SO_2 rovibrational energy levels: using quantum theory to extract rotational constants

Praveen Kumar & Bill Poirier

To cite this article: Praveen Kumar & Bill Poirier (2019): Isotope shifts and band progressions in SO_2 rovibrational energy levels: using quantum theory to extract rotational constants, Molecular Physics, DOI: 10.1080/00268976.2019.1567850

To link to this article: https://doi.org/10.1080/00268976.2019.1567850

Published online: 13 Jan 2019.

MOLECULAR PHYSICS
https://doi.org/10.1080/00268976.2019.1567850

Taylor & Francis
Taylor & Francis Group

ARTICLE

Isotope shifts and band progressions in SO_2 rovibrational energy levels: using quantum theory to extract rotational constants

Praveen Kumar [a] and Bill Poirier[a,b]

[a]Department of Chemistry and Biochemistry, Texas Tech University, Lubbock, Texas, 79409-1061; [b]Max-Planck-Institut für Physik komplexer Systeme, Dresden, Germany

ABSTRACT

We report the isotope shifts of the rotational constants and vibrational band progressions of the sulfur dioxide molecule (SO_2), for all four stable sulfur isotopes ^{32}S,^{33}S,^{34}S, and ^{36}S. These are extracted from exact quantum theoretical calculations of the SO_2 rovibrational energy levels, as reported in *Chem. Phys.* **450–451**, 59 (2015) and *Chem. Phys.* **461**, 34 (2015) and by fitting these levels to a *J*-shifting (JS)-type scheme, applied to a representative set of total angular momentum (*J*) values. The approach used to obtain the rotational constants is unusual in that it is derived directly from the quantum theoretical framework used for the earlier calculation, which gives rise to a flexible (i.e., vibrational- and rotational-state-dependent) but *symmetric* rotor description. The usual (K_a, K_c) rotational quantum numbers are thus replaced with a single body-fixed azimuthal rotation quantum number, *K*, with various strategies introduced *a posteriori* to address rotor asymmetry. The new model fits the numerically computed rovibrational levels well, over a fairly broad range of vibrational (*v*) and rotational (*J*) excitations. The computed rotational constants agree well with previously reported experimental values [*J. Chem. Phys.* **58**, 265 (1973)]. The explicitly *v*- and *J*-dependent approach used here should thus prove valuable in broader contexts—e.g., for an analysis of self-shielding in sulfur mass-independent fractionation, even though the rovibrational levels themselves exhibit mass-dependent fractionation.

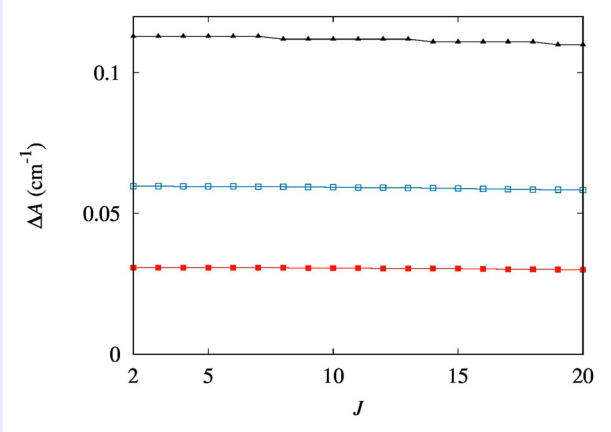

ARTICLE HISTORY
Received 18 October 2018
Accepted 20 December 2018

KEYWORDS
SO_2 isotopologue; Mass-independent fractionation; Rotational constant; Self-shielding; *J*-shifting

1. Introduction

The rovibrational spectroscopy of the sulfur dioxide (SO_2) molecule is of great interest in a variety of disciplines. In addition to geochemistry, these include allied fields such as astrobiology, astrophysics, atmospheric science, and planetary science [1–37] as well as more distant fields. Among other current challenges, highly accurate knowledge of the rovibrational energy levels of SO_2—across all stable sulfur isotopologues, and with reliable quantum number label assignments—may be very useful for resolving one of the most important unsolved mysteries currently facing the geochemistry community: the origin of the sulfur mass-independent fractionation (S-MIF) observed in the Archean rock record [10,22,27,31,38–52]. More specifically, the dramatic and sudden disappearance of the Archean S-MIF signal about

CONTACT Praveen Kumar Praveen.Kumar@ttu.edu Department of Chemistry and Biochemistry, Texas Tech University, Lubbock, Texas, 79409-1061

2.4 Gya—coinciding with the 'Oxygen Revolution'—has sparked great interest in understanding both the signal's origin and its dissolution.

The exact origin of S-MIF signal—as it is observed in the geological record—is likely complicated, and still under debate. A detailed discussion is beyond the scope of this article, although the interested reader is referred to a recent review article [53]. Briefly, it has been suggested that the production and transfer of the S-MIF signal to Archean samples stemmed from an atmospheric photochemistry source that is quenched in an oxygen-rich atmosphere. In Ref. [6], Farquhar et al. proposed the ultraviolet (UV) photodissociation of gas-phase SO_2—which is still considered to be the most likely source. UV absorption leads to SO_2 photodissociation in the range

$$SO_2 + h\nu(165\text{–}220\ \text{nm}) \rightarrow SO + O, \qquad (1)$$

which also corresponds to the Schumann-Runge absorption bands in O_2. Moreover, S-MIF has been observed to arise from SO_2 photodissociation in photocell and other broadband light experiments [43,48,54], although the nature of the S- MIF observed in photocells is of a qualitatively different character than that in the rock record.

In any event, the observed S-MIF signal provides a wealth of potentially extremely revealing information beyond simply the presence or absence of S-MIF. In particular, the observed correlation between $\delta^{34}S$ and $\Delta^{33}S$ [the so-called 'Archean Array' [26], and the (occasional) inverse correlation between $\Delta^{33}S$ and $\Delta^{36}S$ [7,8,19,25] demand a more precise explanation [40,53]. With regard to SO_2 photodissociation, several specific mechanisms have been proposed and/or investigated. At least three involve—as the first step—photoexcitation to the third excited singlet electronic state ($\tilde{C}^1B_2 \leftarrow \tilde{X}^1A_1$) induced by UV photon absorption in the 190 to 220 nm range [3,9,55–59]. Despite some recent suggestions to the contrary [53,55], S-MIF could still arise from any or all of the following:

(1) *Predissociation*, involving an avoided crossing with the $\tilde{D}^1A_1$ singlet electronic state [60–62].
(2) *Intersystem crossing*, with the $\tilde{d}^3A_1$ repulsive triplet electronic state [52,54,60–64].
(3) *Self shielding*, which depends on the availability of UV light of very specific wavelengths near the Earth's surface [29,46,47,55,63,65–67].

The self-shielding argument (3. above) suggests that because ^{32}S is 95% abundant, an SO_2-containing atmosphere might absorb all photons at wavelengths that lead to $^{32}SO_2$ photolysis (i.e., be optically thick) yet not be optically thick at wavelengths that cause photolysis of $^{33}SO_2$, $^{34}SO_2$, and $^{36}SO_2$.

Whether to validate—or to completely rule out—the mechanisms above (especially self shielding), as candidates for geological S-MIF, requires a detailed elucidation of the SO_2 rovibrational energy levels on the ground and excited electronic states, at a level of precision that unambiguously resolves rotational splittings and isotope shifts. This is because the $\tilde{C}^1B_2 \leftarrow \tilde{X}^1A_1$ photoabsorption spectrum exhibits sharp 'fine structure' features, the placement of which is shifted slightly (by several cm^{-1}) via isotopic substitution. In principle, the requisite high-resolution spectra may be obtained either experimentally or theoretically. Indeed, an extensive body of rovibrational experimental data already exists for SO_2, e.g. as deposited in the HITRAN (HI-resolution TRANsmission molecular absorption) database [1,20,23,68–97]. That said, HITRAN and other high-resolution data is still very limited for the rare isotopologues, $^{33}SO_2$ and $^{36}SO_2$—although, since the time of this writing, new $^{33}SO_2$ data has just become available [71,76], and new high-resolution UV photoabsorption spectra for all four isotopologues are currently being obtained [55].

In any event, for the present project, we use only theoretical *ab initio* data, because: (a) it is equally available for all four sulfur isotopologues; (b) there are no 'gaps' in the rovibrational spectral data; (c) the data is uniformly 'clean,' as it all comes from a single source. Recently, we published comprehensive rovibrational level data for all four sulfur isotopologues of SO_2 in Refs. [65] or 'Paper I' and [66] or 'Paper II'—with higher accuracy than previous calculations, and providing symmetry and rovibrational labels for every computed state. The rovibrational energy levels were computed using the ***ScalIT*** suite of parallel codes [98–101]. All rovibrational levels were computed on the ground electronic state, $\tilde{X}^1A_1$, using the empirical, full variational potential energy surface (PES) of Kauppi and Halonen [102]. At the time, this PES provided the best agreement with experiment [14,36,65,66,103,104], although several improved PESs have since become available [14,61,105]. All rovibrational energy levels were obtained using spectroscopically accurate ($10^{-5}\ cm^{-1}$) quantum theory—i.e., no approximations beyond Born-Oppenheimer were employed, and in particular, all rotation-vibration coupling was treated exactly.

The goal of this paper is to extract rovibrational-state-dependent SO_2 rotational constants from the theoretical rovibrational data obtained in Paper I and Paper II—in a way that may be meaningful across the full range of rotational and vibrational excitation that is relevant for the S-MIF mechanisms discussed above. Rotational constants are helpful for making sense of spectra; in

particular, they can be used to assign individual rotational (J_{K_a,K_c}) and vibrational [$v = (v_1 v_2 v_3)$] quantum number labels, which neither experiment nor quantum theory can provide directly on its own. They can also be used to *predict* unobserved (or uncomputed) rovibrational levels—although only to a lower level of accuracy. For the present purpose, fine-structure resolution is required—i.e., on the order of 1 cm^{-1}. It should be noted that this level of accuracy is consistent with that of the PES used.

In general terms, the assignment of separate rotational and vibrational quantum numbers can be achieved using some approximate model of the rovibrational spectrum that assumes additively separable contributions for the rotational and vibrational energy. For our purposes, we refer to any such model as a 'J-shifting (JS) model' [106–108], even though traditionally, this language has been reserved for the reaction scattering context. Generally speaking, the rotational energy contribution is determined from three rotational constant parameters. In the traditional approach, the rotational constants for a molecule are obtained classically, from its equilibrium geometry. The assumption is that of the 'classical rigid rotor'—i.e., that the molecule spends none of its time exploring other geometries. The classical rigid rotor model tends to work best when there is little rotational and vibrational excitation, so that $J \approx 0$ and $v \approx 0$. For a broader range of J and v however, this choice is generally not the best.

For bent triatomic molecules such as SO_2, the classical rigid rotor is necessarily *asymmetric* (all three rotational constants are different). In reality, however, the true quantum molecule can exhibit far less asymmetry than predicted classically. The reason is that in the quantum context of 'semirigid' molecules, the geometry is not fixed but 'vibrationally averaged' [109] (i.e., averaged over the range of geometries available to a given vibrational state). Indeed, the quantum theoretical framework used to compute the rovibrational levels in Papers I and II, *itself* suggests a JS model for which the rotational contribution always corresponds to a *symmetric* rotor. Moreover, this choice has been shown to lead to substantially improved performance over other JS models, when considering a range of J and v values [107]. Accordingly, in this paper, we apply the symmetric JS model to the rovibrational energy levels of Papers I and II, and systematically evaluate whether the resultant fits and assignments are of sufficient quality to address the various mechanisms proposed for S-MIF, such as self shielding. We also improve upon the existing symmetric JS model by developing a *a posteriori* schemes for addressing rotor asymmetry—which in the present context, manifests as 'K-doublet' [109] (or 'lambda-doublet,' [66]) splitting of the doubly-degenerate symmetric-rotor energy levels. Some of these schemes are implemented here, while one is reserved for future work.

2. Theory and computational details

According to experiment [84,110], the equilibrium geometry for SO_2, in its $\tilde{X}^1A_1$ ground electronic state, is a bent structure belonging to the C_{2v} point group, as indicated in Figure 1. Specifically, the O-S-O bond angle is 119.3 °, and each S-O bond length is 1.43 Å. The corresponding classical rigid rotor exhibits fairly little asymmetry, and is otherwise a highly prolate, nearly symmetric rotor. The three principal axes of rotation, (a, b, c), are also indicated in Figure 1. These are associated, respectively, with the three rotational constants (A, B, C), with $A > B > C$. Additionally, the fact that the rotor is highly prolate and nearly symmetric implies that

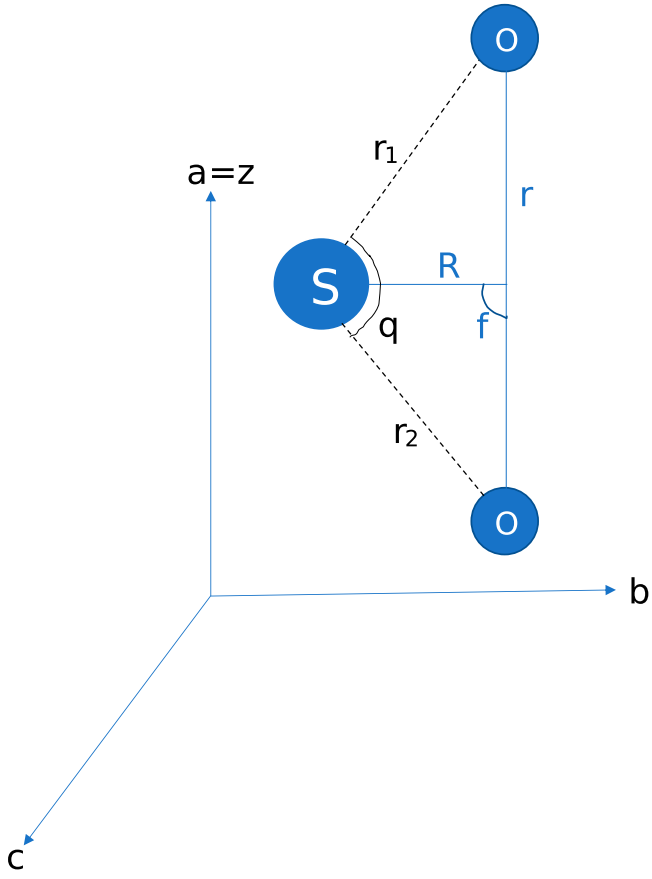

Figure 1. Three-body SO_2 system, as represented in both valence bond and Jacobi coordinates. Valence bond coordinates (r_1, r_2, θ): r_1 and r_2 are the two SO bond distances, and θ is the angle between the two chemical bonds. Jacobi coordinates (r, R, ϕ): r is the distance between the two O atoms, R is the distance between S atom and the O–O centre of mass, and ϕ is the angle between the two vectors associated with r and R. The three principal axes associated with rotational motion, a, b, and c, are also indicated.

Table 1. Various data for the SO_2 molecular system.

Mass	Geometry	$^{32}SO_2$ RC	$^{33}SO_2$ RC	$^{34}SO_2$ RC	$^{36}SO_2$ RC	$^{32}SO_2$ RC (Ref. [73])
$^{16}O = 15.99491462$	$r_1 = 1.4308$ Å	2.018782	1.988178	1.959459	1.906634	$A = 2.027355$
$^{32}S = 31.97207100$	$r_2 = 1.4308$ Å	0.345547	0.345547	0.345547	0.345547	$B = 0.344172$
$^{33}S = 32.97145876$	$\theta = 119.33$ deg	0.295045	0.294383	0.293745	0.292530	$C = 0.293530$
$^{34}S = 33.96786690$						
$^{36}S = 35.96708076$						

Column I: masses for ^{16}O, and for the four stable isotopes of S, as used throughout this paper (atomic mass units). Column II: equilibrium geometry in valence bond coordinates (units listed), for SO_2 in the ground electronic state $\tilde{X}^1A_1$, as determined by experiment (Ref. [110] see also Figure 1). Columns III–VI: classical rigid rotor rotational constants (RC), for the geometry and masses from the first two columns, for all four stable sulfur isotopologues of SO_2 (cm^{-1}). Column VII: experimental $^{32}SO_2$ RC values (cm^{-1}).

$A \gg B \approx C$; the actual numerical values are given in Table 1.

The quantum Hamiltonian for the asymmetric rigid rotor,

$$\hat{H}_{\rm rot} \propto A\hat{J}_a^2 + B\hat{J}_b^2 + C\hat{J}_c^2, \tag{2}$$

provides a useful description of the rotational contribution to the rovibrational energy levels. In Equation (2) above, (A, B, C) are the rotational constants, whereas $(\hat{J}_a, \hat{J}_b, \hat{J}_c)$ are the associated body-fixed components of the angular momentum vector. The eigenvalues of $\hat{H}_{\rm rot}$—i.e., the rotational energies, $E^{\rm rot}_{JK_aK_c}$—are then added to the pure vibrational energy eigenvalues, E_v, to obtain approximate rovibrational energies:

$$E_{vJK_aK_c} \approx E_v + E^{\rm rot}_{JK_aK_c}. \tag{3}$$

In Equation (3) above, the quantum numbers K_a and K_c correspond roughly to rotational excitations about the a and c principal axes, respectively. In general, however, these are not rigorously good quantum numbers.

The asymmetric rigid rotor energy levels, $E^{\rm rot}_{JK_aK_c}$, are known as functions of (A, B, C), but are generally rather complicated. In particular, it can be difficult to extract a quantitative understanding of the nearly-degenerate doublets that arise. A substantial simplification results if prolate symmetric rotational constants are used—i.e., $B = C$. In this case, we find

$$\begin{aligned} E^{\rm JS}_{vJK} &= E_v + E^{\rm rot}_{JK} \\ &= E_v + BJ(J+1) + (A-B)K^2, \end{aligned} \tag{4}$$

where $E^{\rm JS}_{vJK}$ is the symmetric JS approximation to the rovibrational energy, $E_{vJK_aK_c}$. Here, J is the total angular momentum quantum number, and $K = K_z \approx K_a$ is rigorously the rotational excitation about the body-fixed z axis (defined by the Jacobi vector r)—which, in the symmetric prolate context, is also the principal axis a (Figure 1).

In the symmetric JS model, individual rotational states are thus labelled (J, K). For a given J, the quantum number K can take on all $(2J + 1)$ integer values from $-J$ to J. Note, however, that the $(J, \pm K)$ states have the same energy, according to Equation (4). Thus, there are only $(J + 1)$ distinct energy levels, all but one of which (i.e., the $K = 0$ level) are doubly degenerate. It is therefore convenient to redefine $K = |K|$, with $0 \le K \le J$ (Paper I and Paper II). Apart from the simplification that it provides, the above symmetric rotor form is significant because *it arises naturally from the quantum theoretical framework used to compute the exact rovibrational levels*, which uses the Jacobi coordinate system indicated in Figure 1. In this context, J is still a rigorous quantum number, and so rotation-vibration coupling manifests as a coupling across different values of K. By removing this coupling from the exact rovibrational Hamiltonian, one obtains independent diagonal (J, K) blocks that adhere to a *symmetric* rotor form. For each such block, the rotational constants depend on geometry, as expected; however, these turn out *not* to be the classical rigid rotor constants, which always correspond to an asymmetric rotor form. Further details are provided elsewhere [65,66,107].

The symmetric rotor rotational constants that appear in the diagonal-block approximation depend on (J, K), as well as on geometry. By averaging over geometry, using the probability density for a given vibrational state, we obtain a set of symmetric rotor rotational constants that depend explicitly on v, as well as (J, K). These constants are thus rotational-state-dependent (RSD) as well as vibrational-state-dependent (VSD), and it is the added RSD flexibility that enables this approach to (partially) incorporate higher-order coupling effects such as centrifugal distortion. Note, however, that even this fully general *ab initio* approach is always limited by symmetry to predicting doubly-degenerate levels for $K > 0$, and singly degenerate levels for $K = 0$. In reality, the true rovibrational energy levels are all singly degenerate—although they often occur in nearly-degenerate doublets. The K-doublet splitting that does arise is thus a manifestation of *inherent* quantum asymmetry, which can be characterised in terms of the discarded K-block coupling contribution [65,66,107].

In practice, rather than applying vibrational averaging, it is simpler to apply a least-squares fit of Equation (4)

directly to the exact rovibrational levels themselves, if one has access to these (as is the case here). There are various ways in which this can be implemented, leading to different symmetric JS models. For instance, one can always identify isolated singlet levels from the exact rovibrational spectrum as corresponding to $K = 0$. By restricting consideration to just these levels, one can obtain rotational constants B that are VSD and partially RSD (i.e., J-dependent) by dropping the last term from Equation (4):

$$E_{vJ0} = E_v + BJ(J+1). \tag{5}$$

Alternatively, VSD B constants can be obtained by fitting Equation (5) across a range of J values. More generally, VSD A and B constants across all the data can be obtained by fitting Equation (4) across a range of J values.

The above VSD approaches were both adopted in Paper II. Specifically, Equation (4) was fit to all SO_2 rovibrational energy levels in the range $J = 1$–15, for each vibrational state $v = (0, v_2, 0)$, with $v_2 = 0 - 2$. (As will be the case in this paper, to get the best fits all computed levels were considered, including those that are physically forbidden due to nuclear spin symmetry). Second, a fit of all of the $v = (0, 0, 0)$ $K = 0$ rovibrational levels in the range $J = 1$–20 to the form of Equation (5) was also performed, to compute the rotational constant B. The rather stark difference in the resultant computed values for the $v = (0, 0, 0)$ B constant underscores the important role of K-doublet splitting for this system. As predicted in Paper II, the magnitude of K-doublet splitting decreases exponentially with K and increases monotonically with J—meaning that it is most pronounced for $K = 0$ at large J, reaching $\approx 10\,\mathrm{cm}^{-1}$ by $J \approx 20$. Physically, this can be explained as follows: for large J and small K, the rotor behaves more like an *oblate* top, and so the ground and first excited states for a given (v, J) are nearly degenerate, rather than the first and second excited states (see Papers I and II for more details). In any event, this behaviour underscores the need to single out the $K = 0$ levels for special treatment, and/or otherwise deal explicitly with the K-doublet splitting.

In this paper, we generalise previous efforts in several important ways, in order to ensure sub-cm^{-1} accuracy in the predicted rovibrational energy levels, across the entire v and J range of interest. To begin with, we introduce J dependence (partial RSD) into the Equation (4) fits of A and B, as discussed above. The added flexibility of an RSD fit has been demonstrated to yield more accurate JS predictions than a pure VSD approach [107,111]. Next, we explore several different strategies, including *a posteriori* fits, for dealing explicitly with the inherent quantum asymmetry—which manifests in the present context in the form of K-doublet splitting.

3. Results and discussion

In this work we focus on SO_2 containing only ^{16}O, but all four stable sulfur isotopes, ^{32}S, ^{33}S, ^{34}S, and ^{36}S, are considered explicitly. The masses used for all atomic species are indicated in Table 1. For each isotopologue, and each v and J value up to $J = 20$, all $(2J + 1)$ computed rovibrational energy levels from Paper I and Paper II (including unphysical states) are fit to the symmetric JS functional form of Equation (4). The energetically ordered set of $(2J + 1)$ levels is presumed to correspond to $K = K_a = 0, 1, 1, 2, 2, \ldots, J, J$ and $K_c = J, J, \ldots, 1, 1, 0$, as per the standard for a prolate symmetric rotor. We call this fitting procedure, which ignores K-doublet splitting, the 'basic procedure.'

3.1. J-shifting and rotational constants

In cases where K-doublet splitting is most significant (i.e., high J and low K), the deviations of the actual rovibrational energy levels from the symmetric JS predictions are largest. They also exhibit an alternating pattern, wherein the $K_a + K_c = J + 1$ levels show negative deviations, and the $K_a + K_c = J$ levels show positive deviations. As discussed in Section 2, in the most extreme cases, the lowest two levels are nearly degenerate—exhibiting nearly oblate behaviour, i.e. $K_c = J$. Thus, the maximum deviations can be on the order of the K-level spacing itself (i.e., up to around $10\,\mathrm{cm}^{-1}$), which is too large for the present purpose. Moreover, because K-doublet splitting decreases exponentially with K (Paper II), the maximum deviations come to dominate the entire root-mean-square (RMS) error, either directly or indirectly. These trends may be observed in Figure 2.

There is therefore a need for dealing with the K-doublet splitting explicitly, at least in cases where this is pronounced. Based on the alternating pattern discussed above, two simple strategies emerge:

(1) Fit the $K_a + K_c = J$ levels to Equation (4) *separately* from the $K_a + K_c = J + 1$ levels.
(2) *Average* the two energy levels in each K-doublet pair, prior to fitting to Equation (4); then model the K-doublet splitting separately.

Both of these strategies are applied and evaluated for SO_2 in this paper, as is the basic strategy that ignores K-doublet splitting altogether. In addition, it turns out that the behaviour of the $K = 0$ singlet level is rather different from the doublets. In order to obtain improved fits, therefore, we also consider variations of the above strategies, for which the $K = 0$ level is isolated from the doublets, and treated separately (for Strategy 2., this is the only variant considered).

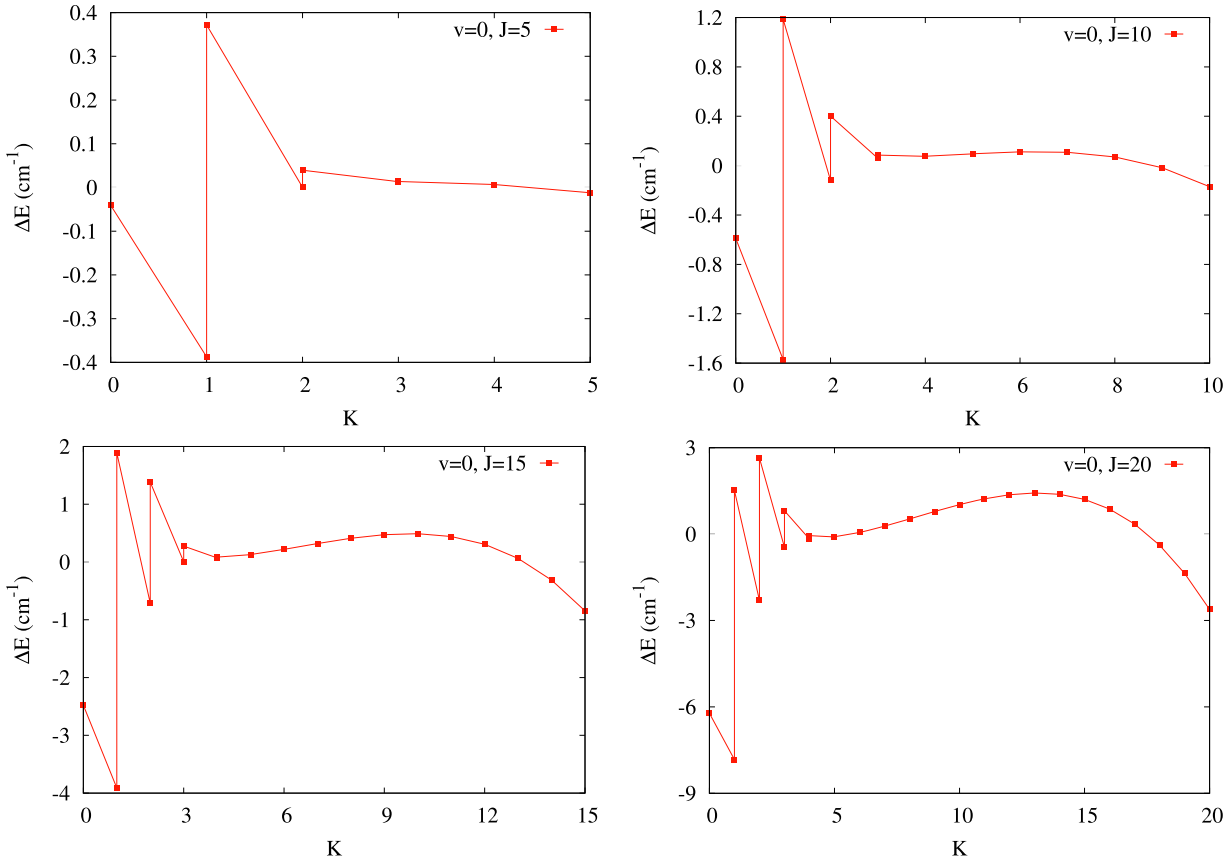

Figure 2. Deviations (ΔE), in cm^{-1}, of the actual rovibrational energy levels as reported in Papers I and II, from the symmetric JS predictions obtained using the 'basic' symmetric JS strategy (i.e., by fitting to $E^{Jshift}_{(0,0,0)JK} = E_{(000)} + BJ(J+1) + (A-B)K^2$) for all $^{32}SO_2$ $v = (0,0,0)$ rovibrational levels, as a function of $|K|$ (red squares, solid line) for $J = 5$, 10, 15 and 20.

In Table 2, we present the root mean square (RMS) deviations obtained when the exact $^{32}SO_2$ $v = (0,0,0)$ rovibrational levels of Paper I and Paper II are fit to Equation (4), using the various strategies described above. All J values from J =1–20 are considered explicitly. The basic strategy, i.e. fitting to all $(2J+1)$ levels together, is represented by Column 2. Likewise, Strategy 1. is considered in Columns 3–6, and Strategy 2 in Column 7 in which reported RMS errors are relative to the centre of each doublet. The primary trend is that RMS deviations increase considerably with increasing J, as expected. We also observe that both strategies above are effective at improving the quality of fits, as evidenced by substantial reductions in RMS deviations. In particular, Strategy 2 is the most effective up to $J = 15$, by far. For the larger J values, Strategy 1 becomes slightly more effective—at least for the $K_a + K_c = J$ levels with the $K = 0$ state removed. The latter modification can alone reduce RMS deviations by up to a factor of two, which again confirms the special role of the $K = 0$ state. As a rule, much greater improvement is observed at the smaller J values (up to 40-fold RMS reduction) than at the higher J values (only 2-fold RMS reduction). In any event, the goal of sub-cm^{-1} accuracy is achieved—e.g., for the $K_a + K_c = J$ fits without $K = 0$. The above trends all hold for the excited vibrational state fits, as well.

In Table 3, we present all rotational constants obtained using Strategy 2 above—for all four sulfur isotopologues of SO_2, for all $(0, v_2, 0)$ vibrational states up to $v_2 = 2$, and for all J =2–20. These relatively low-lying rovibrational states are the most relevant for self shielding. The rotational constant A is about six times larger than B, reflecting the highly prolate nature of the SO_2 molecule. Various trends in the rotational constant values are evident from the table, with respect to varying the isotopologue, v, or J. In particular, the values of both A and B decrease monotonically with increasing mass of the S atom, in a manner that corresponds to a mass-dependent fractionation (MDF) pattern in the SO_2 rovibrational energy levels. Note, however, that the value of A is *much* more strongly dependent on isotopologue than is B, even in a relative sense ($\approx$6% vs. $\approx$0.4%). The effect on A and B of increasing the bend vibrational excitation is similar to that of varying the sulfur isotope; however, this

Table 2. RMS deviations, in cm^{-1}, obtained by fitting the exact $^{32}SO_2$ $v = (0, 0, 0)$ rovibrational energy levels (Paper I and Paper II) to the symmetric JS form of Equation (4), for each J value in the range $1 \leq J \leq 20$.

	Basic	Strategy 1				Strategy 2
	All K	$K_a + K_c = J + 1$		$K_a + K_c = J$		K-doublet-averaged
J	With $K = 0$	With $K = 0$	Without $K = 0$	With $K = 0$	Without $K = 0$	Without $K = 0$
1	2.07E−02					
2	4.80E−02	3.39E−02		3.34E−02		
3	0.081287	5.86E−02	4.49E−02	6.05E−02	4.09E−02	2.01E−03
4	0.119705	9.00E−02	8.48E−02	9.19E−02	7.41E−02	5.38E−03
5	0.163007	0.128187	0.130343	0.128283	0.135997	1.11E−02
6	0.211285	0.173378	0.182016	0.169027	0.143106	2.00E−02
7	0.264922	0.226464	0.240445	0.214460	0.177795	3.29E−02
8	0.324562	0.288743	0.306237	0.265270	0.211883	5.10E−02
9	0.391172	0.361790	0.380083	0.322722	0.247918	7.53E−02
10	0.465862	0.447322	0.462784	0.388213	0.277535	0.107228
11	0.549964	0.547220	0.555414	0.463427	0.309498	0.148112
12	0.644654	0.663023	0.686157	0.549624	0.341671	0.199491
13	0.751252	0.796275	0.774693	0.648116	0.375401	0.263046
14	0.871013	0.948306	0.903970	0.759931	0.412640	0.340541
15	1.005330	1.120420	1.048340	0.886196	0.456152	0.433934
16	1.155690	1.313840	1.209480	1.028060	0.509660	0.545269
17	1.323720	1.529810	1.389170	1.186950	0.577527	0.676647
18	1.511280	1.769670	1.589290	1.364630	0.664572	0.830237
19	1.720450	2.034860	1.811910	1.563150	0.775462	1.008240
20	1.953460	2.326970	2.059150	1.784800	0.914314	1.212870

Various fitting strategies are employed, in an attempt to deal with K-doublet splitting (Section 3.1).

causes an *increase* rather than a decrease in A, due presumably to the fact that the molecule can now better explore geometries closer to a linear shape. Finally, varying J has the smallest effect on the A constant, causing a reduction by only 1% or so as J increases from $J = 2$ to $J = 20$. On the other hand, this has the largest impact on B, increasing this value by 1% over the same J range. The J trends reflect centrifugal distortion effects: rotation distorts the molecule's geometry, in a way that may vary its shape with K, but generally increases its size as J increases.

Rotational constants for $^{32}S^{16}O_2$ have been reported previously on many occasions [14,36,65,66,73,84,105,110]. The simplest theoretical rotational constants, based on the classical rigid rotor, have already been presented here in Table 1. The table also lists a set of values obtained by fitting a model with explicit centrifugal distortion contributions directly to experimental (microwave and infrared) data [73]. Of course, these estimates are based on the asymmetric rotor; in order to enable comparisons with the present results, we average the two small rotational constants, B and C. In the case of the experimental data, the results are remarkably close to those presented here for the lowest $v = 0$ and $J = 2$ states—i.e., $A = 2.027355\,cm^{-1}$ from experiment vs. $A = 2.028710\,cm^{-1}$ (Table 3 Column 3 Row 1), and $B = 0.318851\,cm^{-1}$ from experiment vs. $B = 0.318947\,cm^{-1}$ (Table 3 Column 7 Row 1). Note that $J = 2$ is the smallest value for which nontrivial data can be obtained, using the present model.

3.2. Isotope shifts and vibrational band progressions

In this section, we present isotope shifts of the (ro) vibrational levels of the SO_2 isotopologues in terms of the rotational constants and band progressions. Such knowledge may be useful for characterising self shielding, and otherwise provides a detailed understanding of the effect of isotopic substitution on the spectroscopic fine structure.

In Table 4, we present the isotope shifts of the rotational constants A and B for all $(0,v_2,0)$ vibrational states up to $v_2 = 2$, and J values up to $J = 20$. The isotope shifts for $^{33}SO_2$, $^{34}SO_2$, and $^{36}SO_2$ relative to the $^{32}SO_2$—i.e., $\Delta A = (A^{32} - A^{33,34,36})$ and $\Delta B = (B^{32} - B^{33,34,36})$, increase monotonically and nearly linearly with the S isotope mass. The isotope shifts thus exhibit a very uniform MDF, which at low J, also increases ($\approx 5\%$ for ΔA, and $\approx 10\%$ for ΔB) nearly linearly with v_2. That said, the magnitude of the isotope shifts is *much* larger for A than for B, by about a factor of 100×. For ΔA, the J dependence is almost negligible, but for ΔB, it is quite pronounced, at least in a relative sense. The J dependence of ΔB is also not monotonic, starting at $3.80\ 10^{-4}\,cm^{-1}$ for $v = (0, 0, 0)$ $J = 2$, decreasing to $3.30\ 10^{-4}\,cm^{-1}$ by $J = 7$, and then increasing again up to $4.00\ 10^{-4}\,cm^{-1}$ by $J = 20$.

In Figure 3 plots (a) and (b), the isotope shifts of the rotational constants for $v = (0, 0, 0)$ SO_2 are presented in graphical form, as a function of J. For completeness,

Table 3. Rotational constants A and $B = C$, in cm^{-1}, obtained by fitting the exact SO_2 rovibrational energy levels (Paper I and Paper II) to the symmetric JS form of Equation (4), using Strategy 2 of Section 3.1 (K-doublet averaging), for all four stable sulfur isotopologues (indicated via superscript), for $v = (0, v_2 \leq 2, 0)$, and for $2 \leq J \leq 20$.

J	v_1, v_2, v_3	A^{32}	A^{33}	A^{34}	A^{36}	B^{32}	B^{33}	B^{34}	B^{36}
2	0,0,0	2.028710	1.997870	1.969020	1.915880	0.318947	0.318567	0.318306	0.317714
	0,1,0	2.071410	2.039870	2.010410	1.956060	0.318589	0.318186	0.317939	0.317347
	0,2,0	2.115560	2.083300	2.053210	1.997630	0.318228	0.317800	0.317589	0.316964
3	0,0,0	2.028320	1.997520	1.968660	1.915540	0.319062	0.318715	0.318427	0.317838
	0,1,0	2.070870	2.039380	2.009900	1.955590	0.318847	0.318487	0.318205	0.317603
	0,2,0	2.114880	2.082680	2.052550	1.997000	0.318623	0.318259	0.317990	0.317371
4	0,0,0	2.027790	1.997020	1.968160	1.915060	0.319189	0.318851	0.318557	0.317965
	0,1,0	2.070300	2.038840	2.009350	1.955070	0.318979	0.318632	0.318335	0.317733
	0,2,0	2.114250	2.082080	2.051950	1.996440	0.318771	0.318412	0.318122	0.317508
5	0,0,0	2.027140	1.996380	1.967540	1.914460	0.319326	0.318994	0.318693	0.318102
	0,1,0	2.069550	2.038120	2.008650	1.954400	0.319142	0.318801	0.318498	0.317897
	0,2,0	2.113420	2.081280	2.051150	1.995690	0.318963	0.318611	0.318312	0.317696
6	0,0,0	2.026350	1.995620	1.966790	1.913760	0.319474	0.319143	0.318840	0.318247
	0,1,0	2.068680	2.037280	2.007820	1.953620	0.319300	0.318961	0.318653	0.318051
	0,2,0	2.112450	2.080350	2.050240	1.994820	0.319132	0.318784	0.318476	0.317862
7	0,0,0	2.025440	1.994730	1.965930	1.912940	0.319633	0.319303	0.318996	0.318403
	0,1,0	2.067670	2.036300	2.006860	1.952710	0.319477	0.319139	0.318828	0.318223
	0,2,0	2.111320	2.079250	2.049170	1.993810	0.319329	0.318981	0.318668	0.318051
8	0,0,0	2.024410	1.993730	1.964950	1.912010	0.319803	0.319471	0.319162	0.318565
	0,1,0	2.066520	2.035180	2.005780	1.951680	0.319660	0.319321	0.319006	0.318398
	0,2,0	2.110040	2.078010	2.047970	1.992670	0.319528	0.319179	0.318861	0.318240
9	0,0,0	2.023260	1.992620	1.963870	1.910980	0.319982	0.319649	0.319336	0.318735
	0,1,0	2.065240	2.033940	2.004570	1.950530	0.319858	0.319516	0.319197	0.318584
	0,2,0	2.108610	2.076630	2.046620	1.991390	0.319745	0.319394	0.319071	0.318443
10	0,0,0	2.021990	1.991390	1.962670	1.909840	0.320170	0.319834	0.319517	0.318911
	0,1,0	2.063830	2.032570	2.003240	1.949270	0.320063	0.319718	0.319395	0.318775
	0,2,0	2.100420	2.075100	2.045140	1.989990	0.321567	0.319615	0.319285	0.318651
11	0,0,0	2.020610	1.990050	1.961370	1.908610	0.320367	0.320028	0.319707	0.319093
	0,1,0	2.062290	2.031080	2.001790	1.947900	0.320282	0.319934	0.319606	0.318978
	0,2,0	2.105330	2.073450	2.043530	1.988460	0.320213	0.319856	0.319520	0.318877
12	0,0,0	2.019120	1.988600	1.959960	1.907270	0.320570	0.320227	0.319900	0.319278
	0,1,0	2.060630	2.029470	2.000220	1.946410	0.320505	0.320152	0.319818	0.319181
	0,2,0	2.103470	2.071650	2.041780	1.986810	0.320458	0.320095	0.319753	0.319099
13	0,0,0	2.017510	1.987040	1.958450	1.905840	0.320780	0.320431	0.320099	0.319468
	0,1,0	2.058840	2.027730	1.998540	1.944820	0.320737	0.320378	0.320037	0.319389
	0,2,0	2.101490	2.069720	2.039910	1.985040	0.320713	0.320343	0.319994	0.319328
14	0,0,0	2.015800	1.985380	1.956830	1.904310	0.320997	0.320642	0.320304	0.319662
	0,1,0	2.056930	2.025890	1.996740	1.943120	0.320976	0.320611	0.320263	0.319603
	0,2,0	2.101300	2.069540	2.039740	1.984870	0.320504	0.320141	0.319798	0.319144
15	0,0,0	2.013980	1.983620	1.955120	1.902690	0.321221	0.320859	0.320515	0.319860
	0,1,0	2.054910	2.023920	1.994840	1.941310	0.321223	0.320850	0.320496	0.319823
	0,2,0	2.101170	2.069410	2.039610	1.984750	0.320333	0.319976	0.319637	0.318990
16	0,0,0	2.012060	1.981750	1.953310	1.900890	0.321451	0.321083	0.320731	0.320192
	0,1,0	2.052770	2.021850	1.992820	1.939400	0.321479	0.321098	0.320736	0.320049
	0,2,0	2.101080	2.069330	2.039530	1.984680	0.320190	0.319836	0.319501	0.318860
17	0,0,0	2.010030	1.979790	1.951400	1.899160	0.321689	0.321312	0.320954	0.320274
	0,1,0	2.050520	2.019670	1.990700	1.937400	0.321742	0.321352	0.320982	0.320281
	0,2,0	2.101030	2.069290	2.039490	1.984650	0.320065	0.319715	0.319381	0.318744
18	0,0,0	2.007910	1.977730	1.949390	1.897270	0.321934	0.321549	0.321183	0.320490
	0,1,0	2.048160	2.017380	1.988480	1.935290	0.322013	0.321615	0.321236	0.320520
	0,2,0	2.105130	2.073300	2.043420	1.988450	0.319515	0.319176	0.318853	0.318234
19	0,0,0	2.005690	1.975570	1.947300	1.895280	0.322186	0.321793	0.321419	0.320712
	0,1,0	2.045700	2.014980	1.986150	1.933090	0.322292	0.321885	0.321498	0.320767
	0,2,0	2.105340	2.073530	2.043670	1.988740	0.319447	0.319107	0.318783	0.318161
20	0,0,0	2.003370	1.973320	1.945110	1.893210	0.322445	0.322045	0.321663	0.320941
	0,1,0	2.043120	2.012490	1.983730	1.930790	0.322579	0.322163	0.321767	0.321020
	0,2,0	2.110890	2.079140	2.049360	1.994600	0.319068	0.318725	0.318396	0.317763

the Figure 3 plots (c) and (d) also present data for the $v = (0, v_2, 0)$ rovibrational states (for $J = 5$), for $v_2 \leq 2$. From the plots, the nearly linear scaling with respect to S isotope mass is very clear—as is the near J- and v_2-independence (although odd dips such as that seen in $B^{32} - B^{36}$ at $J = 16$ are sometimes also observed in the other, vibrationally excited states as well). These trends are quite relevant, vis-à-vis strategies that have been adopted in the past to address self shielding. Historically, high resolution data for the $\tilde{C}^1B_2 \leftarrow \tilde{X}^1A_1$ photoabsorption spectrum was available only for the $^{32}SO_2$ isotopologue. For the other isotopologues, fine-structure features from the $^{32}SO_2$ spectrum were simply 'translated' by known vibrational band origin isotope shifts [46,47,55,57]. The

Table 4. Rotational constant isotope shifts, $\Delta A = (A^{32} - A^{33,34,36})$ and $\Delta B = (B^{32} - B^{33,34,36})$, in cm^{-1}, obtained from the *K*-doublet-averaged rotational constants of Table 3, for $v = (0, v_2 \leq 2, 0)$, and for $2 \leq J \leq 20$.

J	v_1, v_2, v_3	$A^{32} - A^{33}$	$A^{32} - A^{34}$	$A^{32} - A^{36}$	$B^{32} - B^{33}$	$B^{32} - B^{34}$	$B^{32} - B^{36}$
2	0,0,0	3.08E−02	5.97E−02	1.13E−01	3.80E−04	6.41E−04	1.23E−03
	0,1,0	3.15E−02	6.10E−02	1.15E−01	4.03E−04	6.50E−04	1.24E−03
	0,2,0	3.23E−02	6.23E−02	1.18E−01	4.28E−04	6.39E−04	1.26E−03
3	0,0,0	3.08E−02	5.97E−02	1.13E−01	3.47E−04	6.35E−04	1.22E−03
	0,1,0	3.15E−02	6.10E−02	1.15E−01	3.60E−04	6.42E−04	1.24E−03
	0,2,0	3.22E−02	6.23E−02	1.18E−01	3.64E−04	6.33E−04	1.25E−03
4	0,0,0	3.08E−02	5.96E−02	1.13E−01	3.38E−04	6.32E−04	1.22E−03
	0,1,0	3.15E−02	6.10E−02	1.15E−01	3.47E−04	6.44E−04	1.25E−03
	0,2,0	3.22E−02	6.23E−02	1.18E−01	3.59E−04	6.49E−04	1.26E−03
5	0,0,0	3.08E−02	5.96E−02	1.13E−01	3.32E−04	6.33E−04	1.22E−03
	0,1,0	3.14E−02	6.09E−02	1.15E−01	3.41E−04	6.44E−04	1.24E−03
	0,2,0	3.21E−02	6.23E−02	1.18E−01	3.52E−04	6.51E−04	1.27E−03
6	0,0,0	3.07E−02	5.96E−02	1.13E−01	3.31E−04	6.34E−04	1.23E−03
	0,1,0	3.14E−02	6.09E−02	1.15E−01	3.39E−04	6.47E−04	1.25E−03
	0,2,0	3.21E−02	6.22E−02	1.18E−01	3.48E−04	6.56E−04	1.27E−03
7	0,0,0	3.07E−02	5.95E−02	1.13E−01	3.30E−04	6.37E−04	1.23E−03
	0,1,0	3.14E−02	6.08E−02	1.15E−01	3.38E−04	6.49E−04	1.25E−03
	0,2,0	3.21E−02	6.21E−02	1.18E−01	3.48E−04	6.61E−04	1.28E−03
8	0,0,0	3.07E−02	5.95E−02	1.12E−01	3.32E−04	6.41E−04	1.24E−03
	0,1,0	3.13E−02	6.07E−02	1.15E−01	3.39E−04	6.54E−04	1.26E−03
	0,2,0	3.20E−02	6.21E−02	1.17E−01	3.49E−04	6.67E−04	1.29E−03
9	0,0,0	3.06E−02	5.94E−02	1.12E−01	3.33E−04	6.46E−04	1.25E−03
	0,1,0	3.13E−02	6.07E−02	1.15E−01	3.42E−04	6.61E−04	1.27E−03
	0,2,0	3.20E−02	6.20E−02	1.17E−01	3.51E−04	6.74E−04	1.30E−03
10	0,0,0	3.06E−02	5.93E−02	1.12E−01	3.36E−04	6.53E−04	1.26E−03
	0,1,0	3.13E−02	6.06E−02	1.15E−01	3.45E−04	6.68E−04	1.29E−03
	0,2,0	2.53E−02	5.53E−02	1.10E−01	3.55E−03	2.28E−03	2.92E−03
11	0,0,0	3.06E−02	5.92E−02	1.12E−01	3.39E−04	6.60E−04	1.27E−03
	0,1,0	3.12E−02	6.05E−02	1.14E−01	3.48E−04	6.76E−04	1.30E−03
	0,2,0	3.19E−02	6.18E−02	1.17E−01	3.57E−04	6.93E−04	1.34E−03
12	0,0,0	3.05E−02	5.92E−02	1.12E−01	3.43E−04	6.70E−04	1.29E−03
	0,1,0	3.12E−02	6.04E−02	1.14E−01	3.53E−04	6.87E−04	1.32E−03
	0,2,0	3.18E−02	6.17E−02	1.17E−01	3.63E−04	7.05E−04	1.36E−03
13	0,0,0	3.05E−02	5.91E−02	1.12E−01	3.49E−04	6.81E−04	1.31E−03
	0,1,0	3.11E−02	6.03E−02	1.14E−01	3.59E−04	7.00E−04	1.35E−03
	0,2,0	3.18E−02	6.16E−02	1.16E−01	3.70E−04	7.19E−04	1.39E−03
14	0,0,0	3.04E−02	5.90E−02	1.11E−01	3.55E−04	6.93E−04	1.33E−03
	0,1,0	3.10E−02	6.02E−02	1.14E−01	3.65E−04	7.13E−04	1.37E−03
	0,2,0	3.18E−02	6.16E−02	1.16E−01	3.63E−04	7.06E−04	1.36E−03
15	0,0,0	3.04E−02	5.89E−02	1.11E−01	3.62E−04	7.06E−04	1.36E−03
	0,1,0	3.10E−02	6.01E−02	1.14E−01	3.73E−04	7.27E−04	1.40E−03
	0,2,0	3.18E−02	6.16E−02	1.16E−01	3.57E−04	6.96E−04	1.34E−03
16	0,0,0	3.03E−02	5.87E−02	1.11E−01	3.68E−04	7.20E−04	1.26E−03
	0,1,0	3.09E−02	6.00E−02	1.13E−01	3.81E−04	7.43E−04	1.43E−03
	0,2,0	3.18E−02	6.15E−02	1.16E−01	3.54E−04	6.89E−04	1.33E−03
17	0,0,0	3.02E−02	5.86E−02	1.11E−01	3.77E−04	7.35E−04	1.41E−03
	0,1,0	3.09E−02	5.98E−02	1.13E−01	3.90E−04	7.60E−04	1.46E−03
	0,2,0	3.17E−02	6.15E−02	1.16E−01	3.50E−04	6.84E−04	1.32E−03
18	0,0,0	3.02E−02	5.85E−02	1.11E−01	3.85E−04	7.51E−04	1.44E−03
	0,1,0	3.08E−02	5.97E−02	1.13E−01	3.98E−04	7.77E−04	1.49E−03
	0,2,0	3.18E−02	6.17E−02	1.17E−01	3.39E−04	6.62E−04	1.28E−03
19	0,0,0	3.01E−02	5.84E−02	1.10E−01	3.93E−04	7.67E−04	1.47E−03
	0,1,0	3.07E−02	5.95E−02	1.13E−01	4.07E−04	7.94E−04	1.52E−03
	0,2,0	3.18E−02	6.17E−02	1.17E−01	3.40E−04	6.64E−04	1.29E−03
20	0,0,0	3.00E−02	5.83E−02	1.10E−01	4.00E−04	7.82E−04	1.50E−03
	0,1,0	3.06E−02	5.94E−02	1.12E−01	4.16E−04	8.12E−04	1.56E−03
	0,2,0	3.17E−02	6.15E−02	1.16E−01	3.43E−04	6.72E−04	1.31E−03

results of the present study suggest that this strategy may not be appropriate. In particular, the observed *rotational* isotope shift of $\Delta A \approx 0.1\,cm^{-1}$ translates to a rovibrational energy level isotope shift *relative to the vibrational band origin*, of up to $\approx 40\,cm^{-1}$ for $J = 20$. This is much larger than the allowable tolerance for a self shielding analysis, which is probably closer to $1\,cm^{-1}$.

In the above analysis, we explicitly considered SO_2 rovibrational states for vibrational excitations of the bending mode, $v = (0, v_2, 0)$, but only up to $v_2 = 2$. As discussed, these lowest-lying vibrational excitations are the most relevant for self shielding, and also the other S-MIF-pertinent dynamical processes discussed in Section 1. Nevertheless, for other dynamical

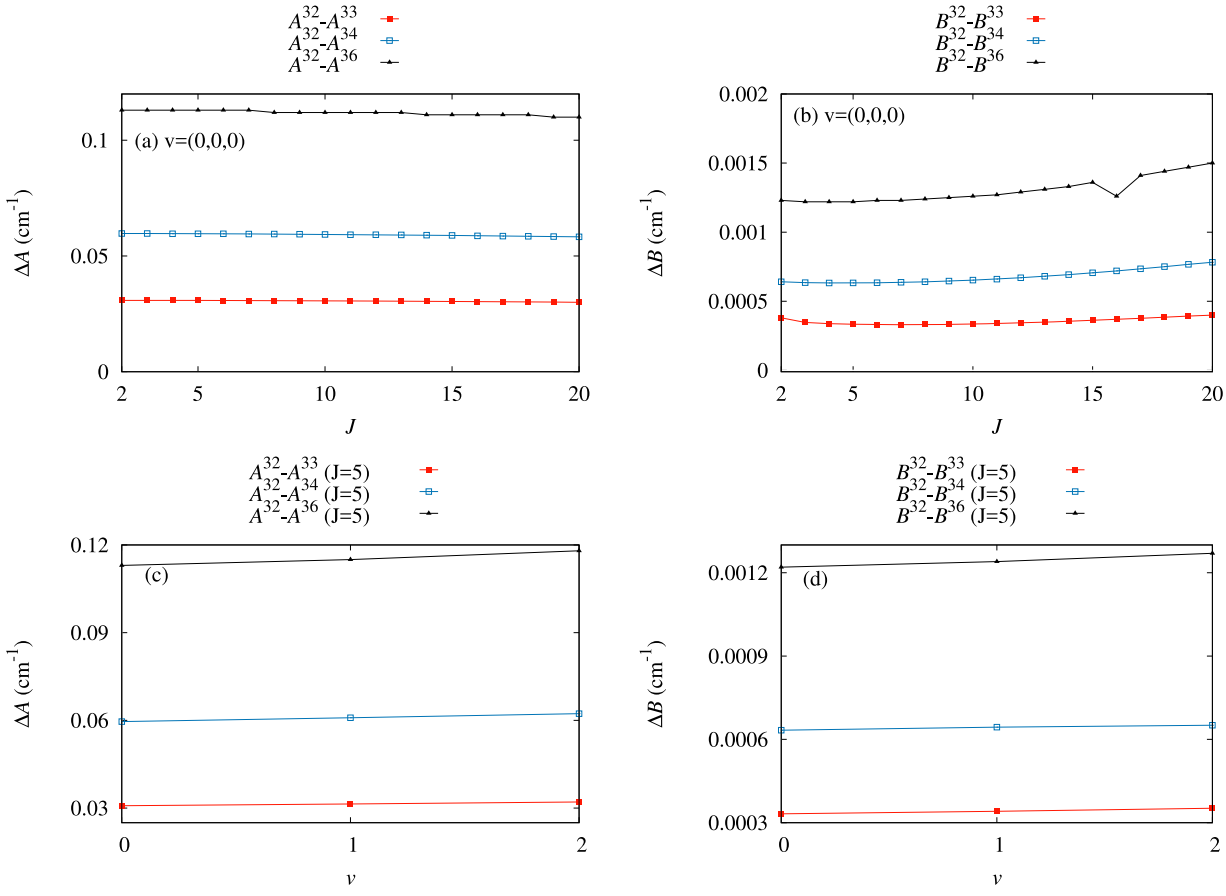

Figure 3. Rotational constant isotope shifts, $\Delta A = (A^{32} - A^{33,34,36})$ [(a), (c)] and $\Delta B = (B^{32} - B^{33,34,36})$ [(b), (d)], obtained from the K-doublet-averaged rotational constants of Table 3: for $v = (0, 0, 0)$ SO_2, as a function of J (top two panels); for $J = 5$ and $v = (0, v_2, 0)$, as a function of v_2. Isotope shifts for all three rare isotopologues are presented, i.e.: $(A^{32} - A^{33})$ (red squares, solid line); $(A^{32} - A^{34})$ (blue empty squares, solid line); $(A^{32} - A^{36})$ (black triangles, solid line); $(B^{32} - B^{33})$ (red squares, solid line); $(B^{32} - B^{34})$ (blue empty squares, solid line); $(B^{32} - B^{36})$ (black triangles, solid line).

pathways, such as fluorescence or collisional stabilisation, the higher-lying vibrational states are also important. Accordingly, we have also analyzed the pure vibrational band progression for the bending mode up to $v_2 = 8$, as well as the symmetric stretch $(v_1, 0, 0)$ and antisymmetric stretch $(0, 0, v_3)$ progressions up to $v_1 = v_3 = 3$. Isotope shifts for the three vibrational band progressions (with band origin shifts obtained from Paper I) are presented in Table 5, for all three rare isotopologues, relative to $^{32}SO_2$. The magnitude of the vibrational progression isotope shifts is largest, by far, for the antisymmetric stretch mode; this is hardly surprising, considering that this mode involves the greatest motion of the S atom. Next is the symmetric stretch mode, followed by the bend. In all cases, isotope shifts are on the order of cm^{-1}'s. They also clearly follow a nearly perfectly linear MDF pattern—meaning that within each row, the numbers in columns 3 and 4 are roughly 2× and 4×, respectively, larger than in column 2.

From Table 5, the isotope shifts within a given vibrational progression are also seen to increase nearly perfectly linearly with vibrational excitation. For each progression and isotopologue but one, the isotope shift is well described by a linear fit of the form $\nu^{32} - \nu \approx \alpha v_i$ cm^{-1} to an RMS deviation no worse than half a cm^{-1}, across the full energetically relevant v_i range considered (i.e., encompassing vibrationally excited states up to $\approx$ 4000 cm^{-1}). Again, this is relevant for a self-shielding analysis, although one does not necessarily expect the same pattern to hold on the $\tilde{C}^1B_2$ electronic state. Indeed, the spectral structure of the $\tilde{C}^1B_2$ vibrational states is known to be highly anomalous, owing primarily to a double well that arises from the asymmetric equilibrium geometry [56,57,63,66]. Furthermore, the most relevant progression for the $(\tilde{C}^1B_2 \leftarrow \tilde{X}^1A_1)$ photoabsorption spectra—which for many years was attributed to $(1, v_2', 2)$—is now known to have a more complicated origin [56,63]. That said, previous work [46,47] has found that this progression exhibits isotope shifts for the

Table 5. Vibrational band progression isotope shifts, $\Delta\nu = (\upsilon^{32} - \upsilon^{33,34,36})$, in cm^{-1}, for the symmetric stretch $(\upsilon_1, 0, 0)$, bend $(0, \upsilon_2, 0)$, and antisymmetric stretch $(0, 0, \upsilon_3)$ modes of SO_2.

$\upsilon_1,\upsilon_2,\upsilon_3$	$\nu^{32} - \nu^{33}$	$\nu^{32} - \nu^{34}$	$\nu^{32} - \nu^{36}$
1,0,0	3.7248	7.2181	13.6348
2,0,0	7.3681	14.2793	26.9775
3,0,0	10.9315	21.1870	40.0343
α	3.6611	7.0955	13.4066
RMS deviation	0.0543	0.1044	0.1945
0,1,0	2.2257	4.3578	8.3920
0,2,0	4.4416	8.6960	16.7454
0,3,0	6.6469	13.0134	25.0582
0,4,0	8.8413	17.3090	33.3284
0,5,0	11.0241	21.5818	41.5540
0,6,0	13.1950	25.8308	49.7327
0,7,0	15.3532	30.0547	57.8623
0,8,0	17.4983	34.2526	65.9406
α	2.1968	4.3006	8.2799
RMS deviation	0.0467	0.0926	0.1815
0,0,1	8.7169	16.9513	32.2353
0,0,2	17.2476	33.5416	55.2345
0,0,3	25.5935	49.7740	90.1675
α	8.5709	16.6683	29.5147
RMS deviation	0.1248	0.2418	2.8541

For each progression and isotopologue, the best linear fit parameter α in $\Delta\nu \approx \alpha\upsilon_i$ is also reported, together with the corresponding RMS deviation.

lower transitions that adhere roughly to the linear form $\delta\nu' = (\nu'^{32} - \nu'^{36}) \approx (20.5 + 7.4\upsilon_2')\ cm^{-1}$, with the other isotopologues following a nearly linear MDF pattern.

Interestingly, the isotope shifts for $(0, \upsilon_2, 0)$ are similar to those above, which may be significant. From a straight energetic perspective (i.e., ignoring Franck-Condon overlaps), the $(0, \upsilon_2, 0)$ vibrational states are most important insofar as hot bands are concerned. On the other hand, when vibrational states of roughly comparable energies are compared—e.g., $(1, 0, 0)$ to $(0, 2, 0)$ and $(0, 0, 1)$ to $(0, 3, 0)$—the υ_1 isotope shifts are found to be smaller than the υ_2 shifts, whereas the υ_3 shifts (and especially RMS deviations) are significantly larger. As discussed in Paper I, this is due to the comparatively greater motion of the S atom in the asymmetric stretch mode vs. the bending mode, or in either of these two modes vs. the symmetric stretch.

4. Summary and conclusions

For a variety of reasons—and across a range of disciplines—it is useful to have an accurate characterisation of the rovibrational states of SO_2, both with respect to the energy levels themselves, and also the rotational (J_{K_a,K_c}) and vibrational $[\upsilon = (\upsilon_1\upsilon_2\upsilon_3)]$ state labels. In the geochemical context, one arena where the SO_2 rovibrational states may be of vital importance is for understanding the S-MIF signal observed in the Archean rock record—assuming that this originates from SO_2 photodissociation. For each of the specific mechanisms described in Section 1, the first step is the $\tilde{C}^1B_2 \leftarrow \tilde{X}^1A_1$ photoabsorption, whose main features (as revealed by experimental spectra) align around vibronic bands spaced roughly $350\ cm^{-1}$ apart. However, in between successive band origins, a very rich fine structure is observed (i.e., at a resolution of $\approx 10\ cm^{-1}$ or smaller), of the sort believed to play an important role in geological S-MIF [53]. Note that the spectroscopic isotope shifts are themselves also on the order of $10\ cm^{-1}$ (Section 3.2).

Many competing factors all play a significant role in determining the fine structure features, including:

- rotational level structure (including J, K, and K-doublet splitting).
- hot bands (i.e. vibrationally excited initial states).
- anomalous vibrational structure of the $\tilde{C}^1B_2$ state.
- less prominent vibronic transitions.
- pressure/third-body effects [48,55].

Disentangling these factors—and assessing the separate impact of isotopic substitution on each—is no small challenge. Building on previous work, in this paper, we make direct contributions to the first two areas above—even though only the ground $\tilde{X}^1A_1$ electronic state is considered, and even though the PES is only accurate to $\approx 1\ cm^{-1}$.

A novel approach is followed, for which the JS (rotor) approximation is suggested by the form of the theoretical Hamiltonian matrix itself, as used in the actual rovibrational state calculation. This choice of JS approximation is unusual in that the resultant rotational constants: (a) do not match the classical rotor geometry; (b) correspond to a *symmetric* rigid rotor; (c) incorporate centrifugal distortion flexibility through VSD *and* (partial) RSD, rather than via higher-order terms added to Equation (2). Nevertheless, the resultant symmetric rotor JS approximation better captures the actual quantum behaviour when there are significant rotational and vibrational excitations.

For the present SO_2 application, the 'basic' symmetric JS strategy described above performs admirably well throughout the relevant ν and J range. However, it is not good enough to achieve the sub-cm^{-1} accuracy desired. This has necessitated the development of the K-doublet (asymmetric level splitting) refinements introduced here, which do indeed achieve the desired accuracy goal. Using the new technique, together with the data from Papers I and II, accurate VSD and RSD rotational constants have been obtained for all of the relevant rovibrational states of $\tilde{X}^1A_1$ SO_2, across all four stable sulfur isotopologues. In each case, isotope shifts were computed, analyzed and then modelled. For the most part, these exhibit standard MDF trends, and are remarkably independent of J. For modelling purposes, however, it is important to keep in mind the following: (a) there *are* some notable

exceptions, that are both J- and isotopologue-specific; (b) even though rotational *constants* may be largely J-independent, the *levels* themselves depend quadratically on J.

These findings have a direct bearing on how the $\tilde{C}^1B_2 \leftarrow \tilde{X}^1A_1$ photoabsorption fine structure ought to be modelled—not only as this pertains to self shielding, but also other aspects related to S-MIF. In the past, comprehensive, reliably accurate high-resolution spectra have been avaliable only for $^{32,34}SO_2$ [9]. Consequently, for modelling the fine-structure features of the rare isotopologues, it has been common practice [46,47,67] to simply red-shift the experimental $^{32}SO_2$ spectrum, based on known isotope shifts for the vibrational bands [57]. The present results suggest that this is a poor strategy—since the rotational contribution to the energy level shifts can be at least as large as the pure vibrational contribution. Nevertheless, these results *do* suggest that reasonably accurate fine structure for the rare isotopologues may indeed be amenable to simple modelling (assuming that other effects such as the last two listed above are not so important). The idea would be to replace the above strategy with one that adopts J-independent shifts of the rotational constants, rather than the levels themselves. Alternatlvely, for greater accuracy, one could simply work directly with the individual rotor constants presented here. Note that a complete description would also require fits for the K-doublet splitting itself, as well as the $K = 0$ states; however, as described previously (Paper II) these are both very predictable and well behaved, and will be considered in future work.

It is noteworthy that the viability of the modelling procedure proposed above could only be confirmed here because of the RSD nature of the approach used; traditional rotational constant fitting procedures do not provide results for individual J values, and can therefore not be used to confirm that isotope shifts are indeed largely J-independent (or conversely, to demonstrate pronounced J dependence, in situations where that is the case). It is also worth mentioning, once again, that high resolution spectra for the rare isotopologues are recently becoming available [55,71,76]. Here too, the techniques used in this paper could be useful, e.g., for identifying individual spectral transitions. In any event, it is anticipated that other researchers may use our comprehensive data, as provided here and in Papers I and II, as a tool for evaluating their own JS schemes, or for modelling various aspects of SO_2 self-shielding and S-MIF.

Acknowledgments

The authors also acknowledge NASA collaborators Millard Alexander, Hua Guo, and Amy Mullin, for many useful discussions. BP also acknowledges support from the Max-Planck-Institut für Physik komplexer Systeme (MPIPKS) Guest Scientist Program. Calculations presented in this paper were performed using the ***ScalIT*** suite of parallel codes.

Disclosure statement

No potential conflict of interest was reported by the authors.

Funding

This work was largely supported by a research grant (NNX13AJ 49G-EXO) from NASA Astrobiology , together with both a research grant (CHE-1665370) and a CRIF MU instrumentation grant (CHE-0840493) from the National Science Foundation (NSF) . The Robert A. Welch Foundation (D-1523) is also acknowledged.

ORCID

Praveen Kumar http://orcid.org/0000-0001-7727-6652

References

[1] G. Ceselin, N. Tasinato, C. Puzzarini, A.P. Charmet, P. Stoppa, and S. Giorgianni, J. Quant. Spectrosc. Radiat. Transf. **203**, 367–376 (2017).
[2] S.O. Danielache, S. Hattori, M.S. Johnson, Y. Ueno, S. Nanbu and N. Yoshida, J. Geophys. Res.-Atmos.**117**, D24301 (2012).
[3] S.O. Danielache, C. Eskebjerg, M.S. Johnson, Y. Ueno and N. Yoshida, J. Geophys. Res. **113**, D17314 (2008).
[4] J. Farquhar, S.T. Kim and A. Masterson, Earth Planet. Sci. Lett. **264**, 1–8 (2007).
[5] J. Farquhar, M. Peters, D.T. Johnston, H. Strauss, A. Masterson, U. Wiechert and A.J. Kaufman, Nature **449**, 706–710 (2007).
[6] J. Farquhar, H. Bao and M.H. Thiemens, Science **289**, 756–758 (2000).
[7] J. Farquhar, J. Savarino, T.L. Jackson and M.H. Thiemens, Geochim. Cosmochim. Acta **64**, 1819–1825 (2000).
[8] J. Farquhar, J. Savarino, T.L. Jackson and M.H. Thiemens, Nature **404**, 50–52 (2000).
[9] D.E. Freeman, K. Yoshino, J.R. Esmond and W.H. Parkinson, Planet. Space Sci. **32**, 1125–1134 (1984).
[10] I. Halevy, M. Zuber and D.P. Schrag, Science **318**, 1903–1907 (2007).
[11] G. Herzberg, *Molecular Spectra and Molecular Structure: Spectra of Diatomic Molecules* (Van Nostrand Reinhold, New York, 1950).
[12] H.D. Holland, Philos. Trans. R. Soc. B **361**, 903–915 (2006).
[13] X. Huang, D.W. Schwenke and T.J. Lee, J. Mol. Spectrosc. **311**, 19–24 (2015).
[14] X. Huang, D.W. Schwenke and T.J. Lee, J. Chem. Phys. **140**, 114311 (2014).
[15] S.S. Johnson, A.A. Pavlov and M.A. Mischna, J. Geophys. Res. **114**, E11011 (2009).
[16] S.S. Johnson, M.A. Mischna, M.T. Zuber and T.L. Grove, J. Geophys. Res. **113**, E08005 (2008).
[17] D.T. Johnston, Earth-Sci. Rev. **106**, 161–183 (2011).

[18] D.T. Johnston, S.W. Puolton, P.W. Fralick, B.A. Wing, D.E. Canfield and J. Farquhar, Geochim. Cosmochim. Acta **70**, 5723–5739 (2006).
[19] A.J. Kaufman, D.T. Johnston, J. Farquhar, A.L. Masterson, T.W. Lyons, S. Bates, A.D. Anbar, G.L. Arnold, J. Garvin and R. Buick, Science **317**, 1900–1903 (2007).
[20] E. Klisch, P. Schilke, S. Belov and G. Winnewisser, J. Mol. Spectrosc. **186**, 314–318 (1997).
[21] K.L. Knappenberger and A.W. Castleman, J. Phys. Chem. A **108**, 9–14 (2004).
[22] S. Martín, J. Martín-Pintado, R. Mauersberger, C. Henkel and S. García- Burillo, Astrophys. J. **620**, 210–216 (2005).
[23] S. Martín, R. Mauersberger, J. Martín-Pintado, S. García-Burillo and C. Henkel, Astron. Astrophys. **411**, L465–L468 (2003).
[24] M.B. Neiman and D. Gál, *The Kinetic Isotope Method and its Application* (Elsevier, Amsterdam, 1971).
[25] S. Ono, A.J. Kaufman and J. Farquhar, Precambrian Res. **169**, 58–67 (2009).
[26] S. Ono, J.L. Eigenbrode and A.A. Pavlov, Earth Planet. Sci. Lett. **213**, 15–30 (2003).
[27] L.E. Snyder, J.M. Hollis, B.L. Ulich, F.J. Lovas, D.R. Johnson and D. Buhl, Astophys. J. **198**, L81–L84 (1975).
[28] H.G. Thode, J. Monster and H.B. Dunford, Geochim. Cosmochim. Acta **25**, 150–174 (1961).
[29] R. Tóbiás, T. Furtenbacher, A.G. Császár, O.V. Naumenko, J. Tennyson, J.-M. Flaud, P. Kumar and B. Poirier, J. Quant. Spectrosc. Radiat. Transf. **208**, 152–163 (2018).
[30] D.S. Underwood, J. Tennyson, S.N. Yurchenko, X. Huang, D.W. Schwenke, T.J. Lee, S. Clausen and A. Fateev, Mon. Not. R. Astron. Soc. **459**, 3890–3999 (2016).
[31] C. Visscher, K. Lodders and B. Fegley, Jr., Sulfur Phosphorus Astrophys. J. **648**, 1181–1195 (2006).
[32] M. Wolfsberg, Annu. Rev. Phys. Chem. **20**, 449–478 (1969).
[33] C.Y.R. Wu, B.W. Yang, F.Z. Chen, D.L. Judge, J. Caldwell and L.M. Trafton, Icarus **145**, 289–296 (2000).
[34] D. Xie, H. Guo, O. Bludský and P. Nachtigall, Chem. Phys. Lett. **329**, 503–510 (2000).
[35] D. Xie, G. Ma and H. Guo, J. Chem. Phys. **111**, 7782–7788 (1999).
[36] K. Yamanouchi, H. Yamada and S. Tsuchiya, J. Chem. Phys. **88**, 4664–4670 (1988).
[37] E.J. Zak and J. Tennyson, J. Chem. Phys. **147**, 094305 (2017).
[38] M.W. Claire, J.F. Kasting, S.D. Domagal-Goldman, E.E. Stueken, R. Buick and V.S. Meadows, Geochim. Cosmochim. **141**, 365–380 (2014).
[39] J.E. Dickens, W.M. Irvine, R.L. Snell, E.A. Bergin, F.P. Schloerb, P. Pratap and M.P. Miralles, Astrophys. J. **542**, 870–889 (2000).
[40] S.D. Domagal-Goldman, B. Poirier and B. Wing, *Summary report from workshop on "Mass-independent Fractionation of Sulfur Isotopes: Carriers and Sources* (2012). < https://nai.nasa.gov/media/medialibrary/2013/08/S-MIF_WorkshopSummary.pdf > .
[41] J. Farquhar, J. Savarino, S. Airieau and M.H. Thiemens, J. Geophys. Res. **106**, 32829–32839 (2001).
[42] J. Farquhar and B.A. Wing, Earth Planet. Sci. Lett. **213**, 1–13 (2003).
[43] H.B. Franz, S.O. Danielache, J. Farquhar and B.A. Wing, Chem. Geol. **362**, 56–65 (2013).
[44] I. Halevy, D.T. Johnston and D.P. Schrag, Science **329**, 204–207 (2010).
[45] J.R. Lyons, Chem. Geol. **267**, 164–174 (2009).
[46] J.R. Lyons, Adv. Quant. Chem. **55**, 57–74 (2008).
[47] J.R. Lyons, Geophys. Res. Lett. **34**, L22811 (2007).
[48] A.M. Masterson, J. Farquhar and J. Wing, Earth Planet. Sci. Lett. **306**, 253–260 (2011).
[49] A.A. Pavlov and J.F. Kasting, Astrobiology **2**, 27–41 (2002).
[50] J. Savarino, A. Romero, J. Cole-Dai, S. Bekki and M.H. Thiemens, Geophys. Res. Lett. **30**, 2131 (2003).
[51] M.H. Thiemens, S. Chakraborty and G. Dominguez, Annu. Rev. Phys. Chem. **63**, 155–177 (2012).
[52] A.R. Whitehill, C. Xie, X. Hu, D. Xie, H. Guo and S. Ono, Proc. Natl. Acad. Sci. USA **110**, 1–6 (2013).
[53] S. Ono, Annu. Rev. Earth Planet. Sci. **45**, 301–329 (2017).
[54] A.R. Whitehill and S. Ono, Geochim. Cosmochim. Acta **94**, 238–253 (2012).
[55] J.R. Lyons, H. Herde, G. Stark, D.S. Blackie, J.C. Pickering and D. de Oliveira, J. Quant. Spectrosc. Radiat. Transf. **210**, 156–164 (2018).
[56] G.B. Park, C.C. Womack, A.R. Whitehill, J. Jiang, S. Ono and R.W. Field, J. Chem. Phys. **142**, 144201 (2015).
[57] H. Ran, D. Xie and H. Guo, Chem. Phys. Lett. **439**, 280–283 (2007).
[58] I. Tokue and S. Nanbu, J. Chem. Phys. **132**, 024301 (2010).
[59] J. Mol. Struct. **352/353**, 541–559 (1995).
[60] B. Jiang, P. Kumar, J. Kłos, M.H. Alexander, B. Poirier and H. Guo, J. Chem. Phys. **146**, 154305 (2017).
[61] J. Kłos, M.H. Alexander, P. Kumar, B. Poirier, B. Jiang and H. Guo, J. Chem. Phys. **144**, 174301 (2016).
[62] C. Xie, B. Jiang, J. Kłos, P. Kumar, M.H. Alexander, B. Poirier and H. Guo, J. Phys. Chem. A **121**, 4930 (2017).
[63] P. Kumar, B. Jiang, H. Guo, J. Kłos, M.H. Alexander and B. Poirier, J. Phys. Chem. A **121**, 1012 (2017).
[64] A.R. Whitehill, B. Jiang, H. Guo and S. Ono, Atmos. Chem. Phys. Discuss. **14**, 23499–23554 (2014).
[65] P. Kumar, J. Ellis and B. Poirier, Chem. Phys. **450-451**, 59–73 (2015).
[66] P. Kumar and B. Poirier, Chem. Phys. **461**, 34–46 (2015).
[67] S. Ono, A.R. Whitehill and J.R. Lyons, J. Geophys. Res. **118**, 2444–2454 (2013).
[68] E. Alekseev, S. Dyubko, V. Ilyushin and S. Podnos, J. Mol. Spectrosc. **176**, 316–320 (1996).
[69] A. Barbe, C. Secroun, P. Jouve, B. Duterage, N. Monnanteuil, J. Bellet and G. Steenbeckeliers, J. Mol. Spectrosc. **55**, 319–350 (1975).
[70] S. Belov, M.Y. Tretyakov, I. Kozin, E. Klisch, G. Winnewisser, W. Lafferty and J.-M. Flaud, J. Mol. Spectrosc. **191**, 17–27 (1998).
[71] T. Blake, J.-M. Flaud and W. Lafferty, J. Mol. Spectrosc. **333**, 19–22 (2017).
[72] M. Carlotti, D. Di Lonardo, L. Fusina, B. Carli and F. Mencaraglia, J. Mol. Spectrosc. **106**, 235–244 (1984).
[73] R.J. Corice, K.J. Fox and G.D.T. Tejwani, J. Chem. Phys. **58**, 265–270 (1973).
[74] G. Crable and W. Smith, J. Chem. Phys. **19**, 502–503 (1951).

[75] Y. Endo, S.O. Danielache, Y. Ueno, S. Hattori, M.S. Johnson, N. Yoshida and G.J. Kjaergaard, J. Geophys. Res.-Atmos. **120**, 2546–2557 (2015).
[76] J.-M. Flaud, T. Blake and W. Lafferty, Mol. Phys. **115**, 447–453 (2017).
[77] G. Guelachvili, O. Naumenko and O. Ulenikov, J. Mol. Spectrosc. **131**, 400–402 (1988).
[78] P. Helminger and F. De Lucia, J. Mol. Spectrosc. **111**, 66–72 (1985).
[79] J. Henningsen, A. Barbe and M.-R. De Backer-Barilly, J. Quant. Spectrosc. Radiat. Transf. **109**, 2491–2510 (2008).
[80] E. Hinkley, A. Calawa, P. Kelley and S. Clough, J. Appl. Phys. **43**, 3222–3224 (1972).
[81] W. Lafferty, J.-M. Flaud, R. Sams and E.H.A. Ngom, J. Mol. Spectrosc. **252**, 72–76 (2008).
[82] W.J. Lafferty, G.T. Fraser, A.S. Pine, J.-M. Flaud, C. Camy-Peyrey, V. Dana, J.-Y. Mandin, A. Barbe, J.J. Plateaux and S. Bouazza, J. Mol. Spectrosc. **154**, 51–60 (1992).
[83] F. Lovas, J. Phys. Chem. Ref. Data **7**, 1445–1750 (1978).
[84] Y. Morino, Y. Kikuchi, S. Saito and E. Hirota, J. Mol. Spectrosc. **13**, 95–118 (1964).
[85] H. Müller, J. Farhoomand, E. Cohen, B. Brupbacher-Gatehouse, M. Schäfer, A. Bauder and G. Winnewisser, J. Mol. Spectrosc. **201**, 1–8 (2000).
[86] H. Müller and S. Brünken, J. Mol. Spectrosc. **232**, 213–222 (2005).
[87] A. Pine, G. Dresselhaus, B. Palm, R. Davies and S. Clough, J. Mol. Spectrosc. **67**, 386–415 (1977).
[88] L.S. Rothman, I.E. Gordon, Y. Babikov, A. Barbe, D. Chris Benner, P.F. Bernath, M. Birk, L. Bizzocchi, V. Boudon, L.R. Brown, A. Campargue, K. Chance, E.A. Cohen, L.H. Coudert, V.M. Devi, B.J. Drouin, A. Fayt, J.-M. Flaud, R.R. Gamache, J.J. Harrison, J.-M. Hartmann, C. Hill, J.T. Hodges, D. Jacquemart, A. Jolly, J. Lamouroux, R.J. Le Roy, G. Li, D.A. Long, O.M. Lyulin, C.J. Mackie, S.T. Massie, S. Mikhailenko, H.S.P. Müller, O.V. Naumenko, A.V. Nikitin, J. Orphal, V. Perevalov, A. Perrin, E.R. Polovtseva, C. Richard, M.A.H. Smith, E. Starikova, K. Sung, S. Tashkun, J. Tennyson, G.C. Toon, Vl.G. Tyuterev and G. Wagner, J. Q. Spectrosc. Radiat. Transf. **130**, 4–50 (2013).
[89] S. Saito, J. Mol. Spectrosc. **30**, 1–16 (1969).
[90] P. Schilke, D. Benford, T. Hunter, D. Lis and T. Phillips, Astrophys. J. Suppl. Ser. **132**, 281 (2001).
[91] K. Takagi and S. Saito, J. Phys. Soc. Jpn. **18**, 1840–1840 (1963).
[92] N. Tasinato, A. Charmet, P. Stoppa, S. Giorgianni and G. Buffa, J. Chem. Phys. **132**, 044315 (2010).
[93] O. Ulenikov, E.S. Bekhtereva, O.V. Gromova, K.B. Berezkin, V.-M. Horneman anf C. Sydow, C. Maul and S. Bauerecker, J. Quant. Spectrosc. Radiat. Transf. **202**, 1–5 (2017).
[94] O. Ulenikov, E. Bekhtereva, O. Gromova, T. Buttersack, C. Sydow and S. Bauerecker, J. Mol. Spectrosc. **319**, 17–25 (2016).
[95] O. Ulenikov, O. Gromova, E. Bekhtereva, I. Bolotova, C. Leroy, V.-M. Horneman and S. Alanko, J. Quant. Spectrosc. Radiat. Transf. **112**, 486–512 (2011).
[96] O. Ulenikov, E. Bekhtereva, O. Gromova, S. Alanko, V.-M. Horneman and C. Leroy, Mol. Phys. **108**, 1253–1261 (2010).
[97] V. Zéninari, L. Joly, B. Grouiez, B. Parvitte and A. Barbe, J. Quant. Spectrosc. Radiat. Transf. **105**, 312–325 (2007).
[98] W. Chen and B. Poirier, J. Parallel Distrib. Comput. **70**, 779–782 (2010).
[99] W. Chen and B. Poirier, J. Comput. Phys. **219**, 185–197 (2006).
[100] W. Chen and B. Poirier, J. Comput. Phys. **219**, 198–209 (2006).
[101] C. Petty, W. Chen and B. Poirier, J. Phys. Chem. A **117**, 7280–7297 (2013).
[102] E. Kauppi and L. Halonen, J. Chem. Phys. **96**, 2933–2941 (1992).
[103] G. Ma, C. Chen and H. Guo, J. Chem. Phys. **110**, 8408–8416 (1999).
[104] G. Ma and H. Guo, J. Chem. Phys. **111**, 4032–4040 (1999).
[105] J. Koput, J. Comp. Chem. **38**, 892–900 (2017).
[106] J.M. Bowman, J. Phys. Chem. **95**, 4960–4968 (1991).
[107] C. Petty and B. Poirier, Chem. Phys. Lett. **605**, 16–21 (2014).
[108] H. Zhang and S.C. Smith, J. Phys. Chem. A **110**, 3246–3253 (2006).
[109] D. Papouvsek and M.R. Aliev, *Molecular Vibrational-Rotational Spectra* (Elsevier Scientific Publishing, Amsterdam, 1982).
[110] Y. Morino, M. Tanimoto and S. Saito, Acta Chem. Scand. A **42**, 346–351 (1988).
[111] B. Poirier, J. Chem. Phys. **108**, 5216 (1988).